Solution structure and fluctuation of the Mg^{2+}-bound form of calmodulin C-terminal domain

Wakana Ohashi, Hiroshi Hirota,* and Toshio Yamazaki*

Genomic Sciences Center, RIKEN, 1-7-22, Suehiro, Tsurumi, Yokohama 230-0045, Japan

Received 24 October 2010; Revised 12 January 2011; Accepted 15 January 2011
DOI: 10.1002/pro.598
Published online 10 February 2011 proteinscience.org

Abstract: Calmodulin (CaM) is a Ca^{2+}-binding protein that functions as a ubiquitous Ca^{2+}-signaling molecule, through conformational changes from the "closed" apo conformation to the "open" Ca^{2+}-bound conformation. Mg^{2+} also binds to CaM and stabilizes its folded structure, but the NMR signals are broadened by slow conformational fluctuations. Using the E104D/E140D mutant, designed to decrease the signal broadening in the presence of Mg^{2+} with minimal perturbations of the overall structure, the solution structure of the Mg^{2+}-bound form of the CaM C-terminal domain was determined by multidimensional NMR spectroscopy. The Mg^{2+}-induced conformational change mainly occurred in EF hand IV, while EF-hand III retained the apo structure. The helix G and helix H sides of the binding sequence undergo conformational changes needed for the Mg^{2+} coordination, and thus the helices tilt slightly. The aromatic rings on helix H move to form a new cluster of aromatic rings in the hydrophobic core. Although helix G tilts slightly to the open orientation, the closed conformation is maintained. The fact that the Mg^{2+}-induced conformational changes in EF-hand IV and the hydrophobic core are also seen upon Ca^{2+} binding suggests that the Ca^{2+}-induced conformational changes can be divided into two categories, those specific to Ca^{2+} and those common to Ca^{2+} and Mg^{2+}.

Keywords: calmodulin; magnesium; conformational exchange; NMR; solution structure

Introduction

Calmodulin (CaM) is a ubiquitous intracellular Ca^{2+}-binding protein that functions predominantly in the integration of Ca^{2+} in signal transduction processes. It is composed of two homologous globular domains (N- and C-terminal domains),[1–4] each consisting of two Ca^{2+} binding motifs, called EF-hand motifs.[5] The EF-hand possesses a helix-loop-strand-helix structure and binds to Ca^{2+} via a 12-residue binding sequence. The binding sequence, which is often referred to as the EF-hand loop, is structurally composed of a loop, a strand and the N-terminal part of an α-helix. Ca^{2+} is chelated by seven oxygens from six residues, at positions 1, 3, 5, 7, 9, and 12 in a pentagonal bipyramidal fashion. The residues at positions 1, 3, and 5 are located in the loop, those at positions 7 and 9 are located in the strand, and the residue at position 12 is located in the helix structure. Ca^{2+} binding to the EF-hand of CaM induces the exposure of the hydrophobic core that provides the interaction site for target molecules, including calcium channel, myosin light chain kinase, CaM kinase, calcineurin, and nitric oxide synthase.[1–9]

Abbreviations: COSY, correlation spectroscopy; EDTA, ethylenediaminetetraacetic acid; HSQC, heteronuclear single quantum correlation; NMR, nuclear magnetic resonance; NOE, nuclear Overhauser effect; NOESY, nuclear Overhauser effect spectroscopy; RDC, residual dipolar coupling; R.M.S.D., root mean square deviation; TOCSY, total correlation spectroscopy.

Additional Supporting Information may be found in the online version of this article.

Grant sponsors: RIKEN Structural Genomics/Proteomics Initiative (RSGI), the National Project on Protein Structural and Functional Analyses, Ministry of Education, Culture, Sports, Science and Technology of Japan.

**Correspondence to:* Toshio Yamazaki, SSBC, RIKEN, 1-7-22, Suehiro, Tsurumi, Yokohama 230-0045, Japan. E-mail: yamazaki@gsc.riken.jp or Hiroshi Hirota, Genomic Sciences Center, RIKEN, 1-7-22, Suehiro, Tsurumi, Yokohama 230-0045, Japan. E-mail: hirota@gsc.riken.jp

Mg^{2+} can also bind to all of the EF-hands of CaM, and shares the same binding site with Ca^{2+}.[10–14] The Mg^{2+} association constants range between 10^2 and 10^4 M^{-1}.[10] Since Mg^{2+} exists in the cytosol at a millimolar concentration,[15] the high affinity sites (EF-hands I and IV) can be converted into the Mg^{2+}-bound forms. The folded structure of CaM is stabilized by Mg^{2+} binding.[13,16] The Mg^{2+}-bound form of CaM is more stable than the apo form of CaM against denaturation by chemicals, such as urea and guanidine, and by thermodynamic effects.[17,18] Mg^{2+} increases the denaturation temperature of each domain of CaM by more than 20°C[18] (Supporting Information Table S1). Mg^{2+} binding seems to be important to stabilize the structure of CaM.

Ca^{2+} and Mg^{2+} cause distinct conformational changes of CaM.[10,12,13] In the Ca^{2+}-bound form, the hydrophobic core is exposed.[1] However, it has been proposed that the hydrophobic core is not exposed in the Mg^{2+}-bound form.[10] The Mg^{2+}-bound structure of the N-terminal domain of soybean calmodulin isoform 4 (sCaM4), which shares about 78% sequence identity with bovine CaM,[19] has been investigated by the backbone residual dipolar coupling approach.[16] The apo form of the N-terminal domain of sCaM4 is unfolded. In the presence of Mg^{2+}, the N-terminal domain of sCaM4 folds into an α-helix-rich structure.[16] This is an excellent example of stabilization by Mg^{2+} binding. The Mg^{2+}-bound form of sCaM4 adopts a closed conformation. Since the structure was calculated by the backbone assignments and the backbone RDC restraints, only the information about the orientation of the EF-hand helices was experimentally determined. Other details, including the Mg^{2+} coordination, the side chain orientations and the arrangement of the hydrophobic core, have remained unknown. To further clarify the details of the Mg^{2+}-induced conformational changes and the features of the Mg^{2+}-bound state, the tertiary structure of the Mg^{2+}-bound form at atomic resolution is needed.

Here, we performed a structural analysis of the Mg^{2+}-bound form of the CaM C-terminal domain (residues 78–148, CaMC) by multidimensional NMR spectroscopy. The two domains (N-terminal domain and C-terminal domain) fold independently, and the Ca^{2+}-binding affinity and the Ca^{2+}-induced structural changes of these domains are both equivalent to those of intact CaM.[18,20] Mg^{2+} preferentially binds to EF-hands I and IV of CaM.[10] In EF-hand I, the Mg^{2+}-induced chemical shift changes are localized in the N-terminal part of the binding sequence.[14] However, in EF-hand IV, the Mg^{2+}-induced changes occur throughout the binding sequence. The NMR signals and the fluorescence intensity of Y138, located on the C-terminal part of the EF-hand IV binding sequence, change upon Mg^{2+} binding.[12,21] Therefore, larger structural changes are anticipated for CaMC.

In an NMR study, the HSQC spectra of the apo and Ca^{2+}-bound forms of CaM displayed well-dispersed signals. On the other hand, the NMR spectra of the Mg^{2+}-bound form of CaM showed signal broadening for most of the residues, indicating that a slow conformational fluctuation, which is an exchange between multiple conformations, occurs around the core of the molecule. NMR signal broadening upon Mg^{2+} binding is a common feature among EF-hand proteins.[22,23] NMR is an appropriate method to monitor the exchange process. The signal broadening problem with the Mg^{2+}-bound form of CaMC was solved by double point mutations. The solution structure of the Mg^{2+}-bound form of CaMC was determined by multidimensional NMR spectroscopy, using the mutant. We observed the structural changes upon Mg^{2+} binding. Although the overall structure was the closed form, like the apo form, most of the structural changes in the binding site and the core region were similar to those induced by Ca^{2+}.

Results

Mg^{2+} induces hydrogen bond interactions in the EF-hand IV loop structure

The glycine residue at position 6 of the binding sequence forms a hydrogen bond between its amide proton and the side chain of the first residue in the binding sequence [Fig. 1(A)].[1] The hydrogen bond is thought to contribute to the formation of the chelating structure. However, the hydrogen bond of EF-hand IV is formed only in the Ca^{2+}-bound state, and is absent in the apo state. Hydrogen bond formation can be monitored by the down-field shift of the amide proton signals in NMR spectra.[24] The signal of G134 (position 6 in EF-hand IV) is detected in the normal shift region in the apo state and shows a large down-field shift upon Ca^{2+} binding.[24] The large down-field shift indicates that Ca^{2+} binding enhances the hydrogen bonding.[24]

To investigate the hydrogen-bond formation in EF-hand IV upon Mg^{2+} binding, the ^1H-^{15}N HSQC spectra of CaMC with and without 10 m*M* Mg^{2+} were recorded. Only the resonance of G98 was detected in the down-field region in the apo state [Fig. 1(B), upper left]. At 10 m*M* Mg^{2+}, the G134 signal of the apo-form disappeared, and a weak down-field signal appeared at a different position from G98 in the apo state [Fig. 1(B), upper right]. The chemical shift of the signal was almost identical to that of G134 in the Ca^{2+}-bound form [Fig. 1(B), lower left]. Therefore, the down-field signal was assigned to G134. This indicates that the hydrogen bond involving the amide proton of G134 is formed upon Mg^{2+} binding. It seems that EF-hand IV is

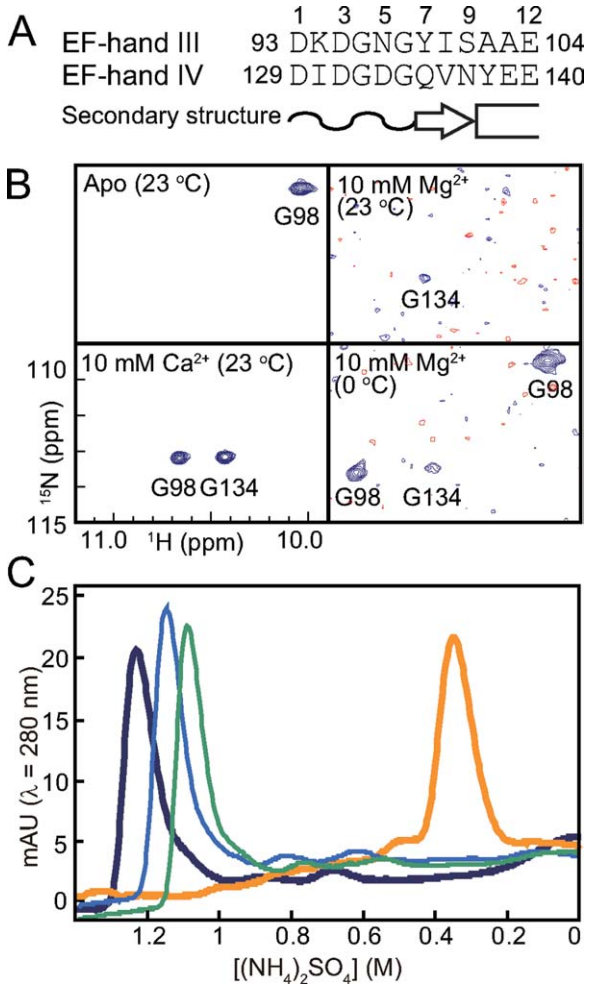

Figure 1. Mg^{2+}-induced and Ca^{2+}-induced changes of CaMC. (A) Primary structure of the EF-hand metal-binding sequences of CaMC (EF-hand III and EF-hand IV). The Ca^{2+} and Mg^{2+} coordinating ligands are indicated by the coordination numbers. The loop structure, the β-strand and the α-helix are indicated as a wavy line, an arrow and a box, respectively. (B) Selected regions of the ^{1}H-^{15}N HSQC spectra of CaMC without Ca^{2+} or Mg^{2+} at 23°C (upper left), with 10 m*M* Mg^{2+} at 23°C (upper right), with 10 m*M* Mg^{2+} at 0°C (lower right) and with 10 m*M* Ca^{2+} (lower left) at 23°C. (C) Hydrophobic interaction column chromatography. The samples were eluted by a concentration gradient of $(NH_4)_2SO_4$ from 2*M* to 0*M*. 0 m*M* (no Mg^{2+} or Ca^{2+} added; green, thin trace), 10 m*M* Mg^{2+} (blue, thin trace), 100 m*M* Mg^{2+} (dark blue, thick trace), 5 m*M* Ca^{2+} (orange, thick trace).

mostly converted to the Mg^{2+}-bound form, although the signal is very weak. (The signal broadening is described below.) In contrast, the signal from G98 disappeared [Fig. 1(B), upper right], suggesting that EF-hand III underwent a conformational exchange between the Mg^{2+}-free and Mg^{2+}-bound states. As previously reported by Ohki *et al.*,[10] EF-hand IV was preferentially occupied by Mg^{2+}, when compared with EF-hand III. In the spectra obtained at a lower temperature, to reduce the exchange rate, two down-field signals appeared in addition to the weak down-field signal of G134 [Fig. 1(B), lower right]. One was the apo-form of G98, and the other was the Mg^{2+}-bound form. This confirmed the assignment of G134 and suggested that the Mg^{2+} is incorporated at least into the position 1 site bonded to position 6. The formation of the hydrogen bond is one of the stabilizing effects of Mg^{2+}-binding.

The hydrophobicity of CaMC is not affected by Mg^{2+} binding

Ca^{2+} binding to CaM induces the exposure of the hydrophobic core on the protein surface, thus increasing the hydrophobicity of the molecule. The effects of Mg^{2+} and Ca^{2+} on the hydrophobicity of CaMC were evaluated by hydrophobic interaction chromatography. As shown in Figure 1(C), the apo form was eluted at $[(NH_4)_2SO_4] = 1.08M$, and the Ca^{2+}-bound form of CaMC displayed a peak at $[(NH_4)_2SO_4] = 0.35M$ in the presence of 5 m*M* Ca^{2+}, indicating that Ca^{2+} binding increased the hydrophobicity of the protein. CaMC was eluted from the column at $(NH_4)_2SO_4$ concentrations of 1.14*M* and 1.2*M* in the presence of 10 m*M* and 100 m*M* Mg^{2+}, respectively [Fig. 1(C)]. Since the Mg^{2+} binding did not increase the hydrophobicity of the protein, the hydrophobic core is probably not exposed by the Mg^{2+} binding.

Conformational exchange among the Mg^{2+}-bound forms of CaMC

The two-dimensional ^{1}H-^{15}N HSQC spectra of the apo and Ca^{2+}-bound forms of CaMC displayed well-dispersed peaks with sharp line widths at 23°C (Fig. 2, upper panels). With 10 m*M* Mg^{2+}, the spectrum showed broadened peaks and fewer signals (Fig. 2, lower left). In the presence of excess (100 m*M*) Mg^{2+}, although some signals were detected, about 30 percent of the signals were missing in the spectrum (Fig. 2, lower right). These results reflect the exchange process between the apo and Mg^{2+}-bound forms, and the additional conformational exchange among the Mg^{2+}-bound structures. It should be noted that the Mg^{2+}-induced broadening of the NMR signals does not represent the instability of the Mg^{2+}-bound form of CaM. As indicated by the thermal unfolding experiment (Supporting Information Table S1), Mg^{2+} binding stabilizes the folding of CaM. The NMR signals of the Mg^{2+}-bound form became sharper at higher temperatures [Fig. 3(A)]. Elevating the temperature increases the exchange rate and provides favorable conditions for observing the Mg^{2+}-bound form by NMR. Although the NMR signals of the Mg^{2+}-bound form became sharper at 50°C, the number of peaks in the HSQC spectrum was still slightly smaller than the expected number, and most of the signals were somewhat broadened.

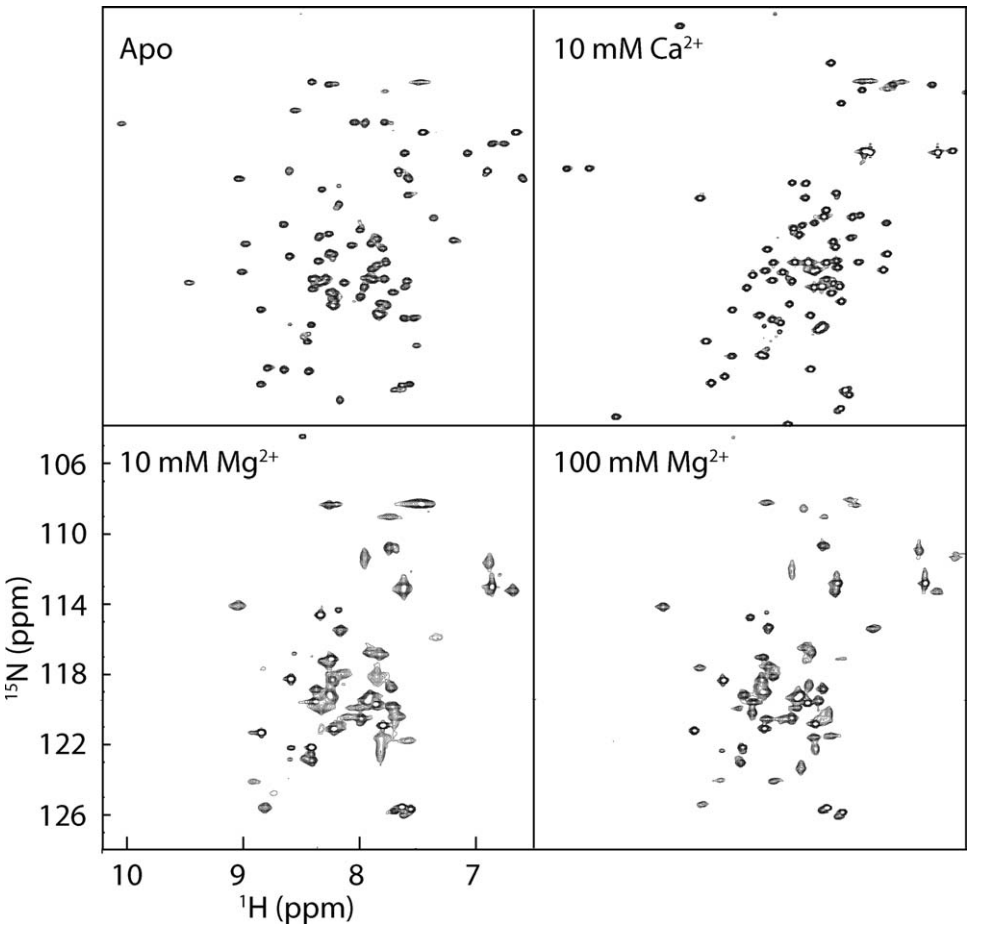

Figure 2. Mg^{2+}-induced exchange broadening. The ^{1}H-^{15}N HSQC spectra of CaMC alone (upper left), with 10 m*M* Ca^{2+} (upper right), with 10 m*M* Mg^{2+} (lower left), and with 100 m*M* Mg^{2+} (lower right) at 23°C.

Conformational exchange converged by point mutations

To improve the behavior of the Mg^{2+}-bound state of CaMC, the E104D, E140D, and E104D/E140D (DD) mutants were constructed. The rationale for introducing these particular mutations was based on the Ca^{2+}/Mg^{2+} binding properties of the EF-hands. E104 and E140 are located at position 12 in each of the EF-hand III and IV binding sequences, respectively [(Fig. 1(A)]. The glutamate is highly conserved at position 12 of the binding sequences. The substitution of aspartate for glutamate in other EF-hand proteins is known to diminish the binding selectivity of Ca^{2+} versus Mg^{2+}.[25–27]

The ^{1}H-^{15}N HSQC spectra of all three mutants are similar to that of the wild type in the apo state at 23°C (data not shown), indicating that the proteins share a similar conformation. The stabilizing effect by Mg^{2+} was also conserved among the mutants (Supporting Information Table S1). Unexpectedly, the HSQC spectra of the apo forms of the E104D and DD mutants were well dispersed even at 50°C, whereas those of the wild type and the E140D mutant were crowded around the middle of the spectrum (Supporting Information Fig. S1). In the apo state, the S101 signals of the E104D and DD mutants were shifted down-field in the ^{1}H-^{15}N HSQC spectra (Supporting Information Fig. S2). The down-field shift can be interpreted as the strengthening of the hydrogen bonding between the backbone amide of S101 and the side chain of E104D. S101 is located just before the helix and is involved in capping of helix F.[2] The N-terminus of helix F is fitted with the capping box motif.[28] The side chain of S101 forms a hydrogen bond with the backbone of E104 and, reciprocally, the side chain of E104 forms a hydrogen bond with the backbone of S101. The capping structure may stabilize helix F, which is known as a fragile helix in the apo state.[18]

The HSQC spectra of the Mg^{2+}-bound form of the DD mutant at 50°C exhibited the best-resolved peaks among the wild type and mutant proteins. The backbone resonances of the Mg^{2+}-bound forms of the wild type and the DD mutant were assigned, and the chemical shifts were compared. The amide chemical shift differences of I130, V136, N137, and Y138 in the EF-hand IV binding sequence were relatively larger than those of the other residues [Fig. 3(A) and Supporting Information Table S2]. To assess whether the DD mutation changes the backbone structures of these

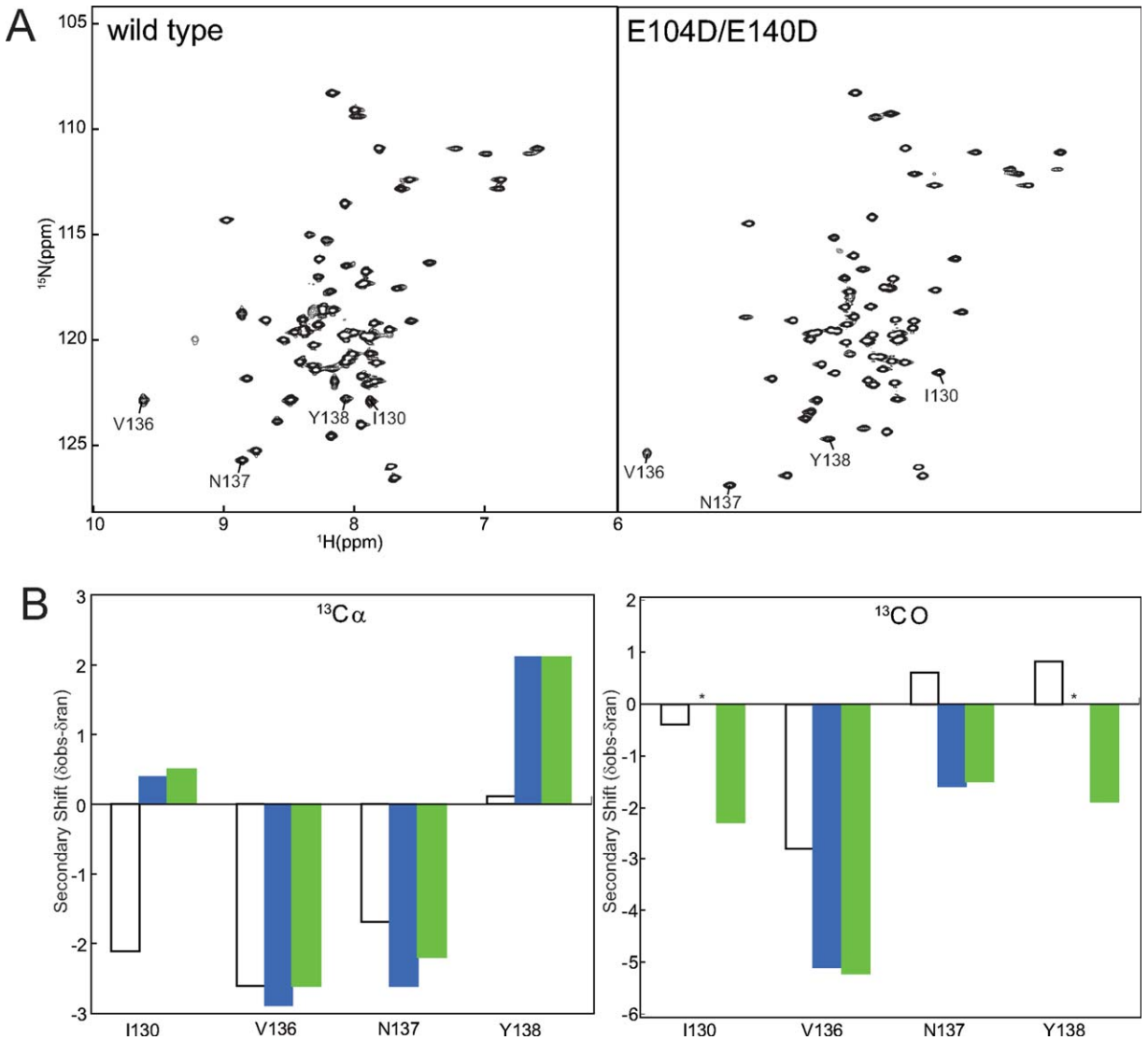

Figure 3. ^{1}H-^{15}N HSQC NMR spectra of Mg^{2+}-bound forms of CaMC wild type and DD mutant. (A) HSQC spectra of CaMC wild type (left) and DD mutant (right) with 100 m*M* Mg^{2+} at 50°C. I130, V136, N137, and Y138 are labeled. (B) Secondary shifts of I130, V136, N137, and Y138 calculated with Cα (left) and CO (right) chemical shifts. Open bars correspond to the shift of the apo form of the wild type, blue bars represent the shift of the Mg^{2+}-bound form of the wild type and green bars indicate the shift of the Mg^{2+}-bound form of the DD mutant. Asterisks show residues with uncalculated secondary shifts, due to the lack of assignment.

residues, the secondary shifts were calculated from the resonances of ^{13}Cα, ^{13}CO, and compared between the Mg^{2+}-bound forms of the wild type and the DD mutant [Fig. 3(B) and Supporting Information Table S2]. These resonances were consistent between the wild type and the DD mutant, indicating that the backbone structures of these residues were essentially retained. The differences in the amide chemical shifts between the wild type and the DD mutant may be explained by the effects of the side chains. In the apo form of the wild type,[3] these resonances differed significantly from those of the Mg^{2+}-bound form, suggesting that Mg^{2+} binding caused the changes in the backbone structures of these residues in the wild type, which were also retained in the DD mutant [Fig. 3(B)]. In other regions, the average chemical shift difference of the Mg^{2+}-bound forms between the wild type and the DD mutant was 0.08, based on the equation described in Figure 4. This is a much smaller difference, when compared with 0.23 for the average chemical shift difference between the apo form and the Mg^{2+}-bound form of the DD mutant. In the wild type, Mg^{2+}-induced down-field shifts of G98 and G134 were observed [Fig. 1(B)]. These down-field shifts were also observed in the DD mutant (data not shown), suggesting that the Mg^{2+} ions were similarly coordinated in EF-hands III and IV of the DD mutant and the wild type. In the ^{13}C NOESY-HSQC spectrum of the wild type, the NOEs were insufficient for the internal residues, including I100 and V136 on the β-sheet. Less broadening of the main chain and side chain signals of I100 and V136 and the surrounding residues was detected

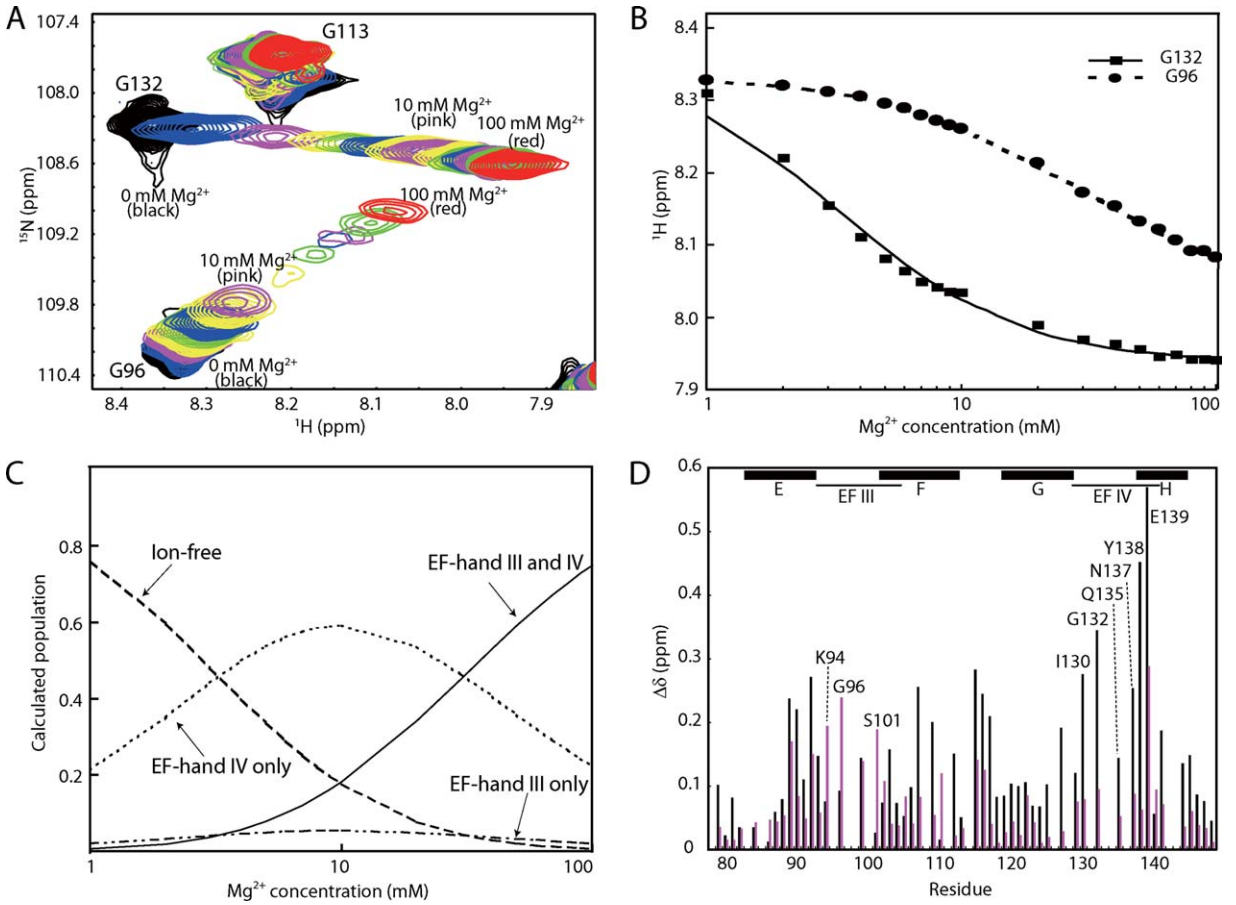

Figure 4. Mg^{2+} binding to the CaMC DD mutant. (A) Titration with Mg^{2+}. Superimposition of the ^{1}H-^{15}N HSQC spectra of the CaMC DD mutant with Mg^{2+} concentrations ranging from 0 to 100 m*M*. Each spectrum was acquired at 50°C. (B) Titration curve for Mg^{2+} binding to the CaMC DD mutant. Amide proton chemical shifts assigned to G96 (EF-hand III, circles) and G132 (EF-hand IV, squares), plotted as a function of the Mg^{2+} concentration. (C) Calculated populations of the different states of the protein, as a function of the Mg^{2+} concentration. The populations were calculated for $K_{III} = 29.4$ m*M*, $K_{IV} = 2.67$ m*M*, and 1 m*M* protein. (D) Backbone amide chemical shift changes induced by Mg^{2+} binding. Black bars represent the chemical shift changes between 0 and 10 m*M* Mg^{2+}, and magenta bars indicate the chemical shift changes between 10 and 100 m*M* Mg^{2+}. The values were calculated with the following equation: $\Delta\delta = \sqrt{\Delta\delta^2 + (\Delta\delta/5)^2}$. The signals of E83, I85, N111, E114, V142, and Q143 were overlapped. The chemical shift changes of the D95, N97, G98, I100, V108, R126, A128, D131, D133, G134, and V136 residues were too broad, and are not included in the plot. The binding sequences of the EF-hands are indicated with a line. The helices are indicated by boxes with their names.

for the DD mutant. More NOE interactions were found, and the total number of NOEs was increased by 35%. A comparison of the ^{13}C NOESY-HSQC spectra of the wild type and the DD mutant revealed that the NOE patterns of the wild type were conserved in the mutant, indicating that the conformation of the mutant predominantly resembled that of the wild type. The wild type may also adopt a minor conformation, and the exchange between them may cause the NMR signal broadening.

The substitution of glutamate with aspartate affects the Ca^{2+} binding potential

The binding potential of the DD mutant for Ca^{2+} was far less than that of the wild type. The Ca^{2+} titration, monitored by NMR, indicated that the DD mutant had a Ca^{2+}-binding constant in the submillimolar range (data not shown). Considering that the wild type binds to Ca^{2+} with a K_d of $\sim 10^{-6}$ *M*, the substitution of glutamate with aspartate decreases the binding potential for Ca^{2+}. The substitution affected the Ca^{2+}-induced change in the hydrophobicity of the protein. The hydrophobic interaction chromatography revealed that the DD mutant with 5 m*M* Ca^{2+} eluted at a similar concentration of $(NH_4)_2SO_4$ to that with either Mg^{2+} or EDTA (Supporting Information Fig. S3). This indicates that the hydrophobic cavity of the DD mutant is not exposed at Ca^{2+}concentrations below 5 m*M*.

Mg^{2+} binding to EF-hand IV has a major impact on the conformational changes of CaMC

The Mg^{2+} titration was performed by recording the ^{1}H-^{15}N HSQC spectra as a function of increasing

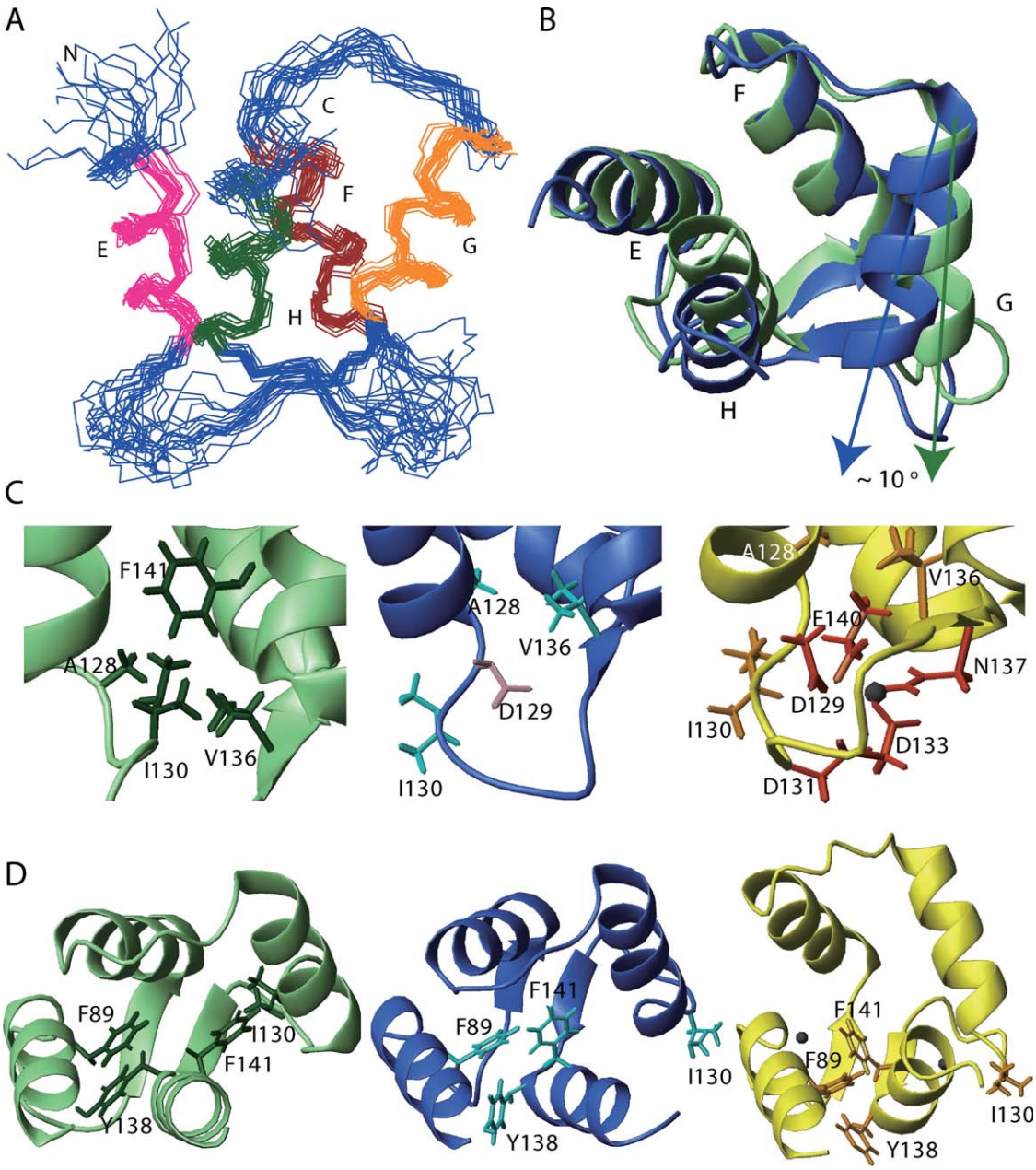

Figure 5. Solution structures of the Mg^{2+}-bound CaMC DD mutant. (A) Ensemble of the backbone heavy atoms of the 20 lowest target functions of the Mg^{2+}-bound form of the CaMC DD mutant. The α-helices are sequentially labeled with letters. Helices E and F form EF-hand III, while G and H form EF-hand IV. (B) Superimposition of the apo form of wild type CaMC (green, PDB ID: 1F71) and the Mg^{2+}-bound form of the CaMC DD mutant (blue). Helices E and F of the apo form are superimposed against the corresponding helices of the Mg^{2+}-bound form. (C) EF-hand IV binding sequence of the apo form of the wild type (left, green), the Mg^{2+}-bound form (center, blue), and the Ca^{2+}-bound form of the wild type (right, yellow, PDB ID: 1J7P) of CaMC. The side chains of A128, I130, V136, and F141 are shown. In the Ca^{2+}-bound form, the side chains of the chelating residues D129, D131, D133, N137, and E140 are shown, and in the Mg^{2+}-bound form, the side chain of the chelating residue D129 is also depicted. The Ca^{2+} ion is shown in black. (D) Ribbon representation of the apo form of the wild type (left, green), the Mg^{2+}-bound form of the DD mutant (center, blue) and the Ca^{2+}-bound form of the wild type (right, yellow) of CaMC. The side chains of F89, I130, Y138, and F141 are also shown.

Mg^{2+} concentration, ranging 0 to 100 m*M*, in 100 m*M* KCl at 50°C for the DD mutant. The NMR signals of the amide protons of G96 (EF-hand III) and G132 (EF-hand IV) during the titration are shown in Figure 4(A). Two glycine residues exist at position 4 in each of the binding sequences and are good probes for Mg^{2+}-binding to these sequences.

The amide chemical shifts of G96 and G132 were plotted as a function of the Mg^{2+} concentration [Fig. 4(B)]. The microscopic Mg^{2+}-binding constants (K_{III}

and K_{IV}) for EF-hands III and IV were calculated using the G96 and G132 data, respectively. EF-hands III and IV bind to two Ca^{2+} ions with positive cooperativity. In contrast, the Mg^{2+}-induced chemical shift changes agreed with the theoretical curve based on the model in which two Mg^{2+} ions bind to the protein independently. The binding manner of Mg^{2+} to the protein was not cooperative. The calculated microscopic Mg^{2+} dissociation constants were K_{III} = 29.4 m*M* and K_{IV} = 2.67 m*M*. Roughly speaking, Mg^{2+} binds to the EF-hands IV and III sequentially, since the binding constants extensively differ. In the presence of 100 m*M* Mg^{2+}, the population of the two Mg^{2+} form is significantly predominant [Fig. 4(C)].

To separate the effects of the binding of the first and second Mg^{2+} ions to the protein, the chemical shift differences between 0 and 10 m*M* Mg^{2+} and those between 10 m*M* Mg^{2+} and 100 m*M* Mg^{2+} were plotted in Figure 4(D). The changes up to 10 m*M* Mg^{2+} mainly reflect the effects of binding to EF-hand IV, and those beyond 10 m*M* Mg^{2+} mainly reflect the binding to EF-hand III. Upon Mg^{2+} binding to EF-hand IV, large chemical shift changes were observed throughout the EF-hand IV binding sequence. The chemical shifts in the EF-hand III binding sequence were predominantly changed upon Mg^{2+} binding to EF-hand III. In all other regions, larger chemical shift changes were observed between 0 and 10 m*M* Mg^{2+}. Even the signals of the F-G linker changed upon Mg^{2+}binding to EF-hand IV, suggesting that either helix F or helix G moved. These results indicated that the first Mg^{2+} binding event to EF-hand IV has a major impact on the structural change.

Solution structure of the Mg^{2+}-bound form of CaMC

We determined the solution structure of the Mg^{2+}-bound form of CaMC, using the DD mutant. Over 90% of the sequence-specific resonance assignments for the polypeptide backbone and the side chains of the Mg^{2+}-bound form of the DD mutant were obtained, through analyses of the 2D and 3D heteronuclear NMR spectra recorded for the uniformly ^{13}C, ^{15}N-labeled protein. The 3D structure of the Mg^{2+}-bound form of the DD mutant was calculated using 840 restraints derived from 1,159 NOEs from 3D NOESY spectra, supplemented with 84 dihedral angles (ϕ, ψ, and χ^1 angles) and 23 hydrogen bonding restraints. Automatic NOE assignments and structure calculations were performed using CYANA 2.2.[29–31] Over 98% of the distance restraints derived from the NOEs were assigned, and the R.M.S.D.s of the backbone atoms of the folded part of the calculated structures were ~0.5 Å. The structural statistics are summarized in Supporting Information Table S3, and the ensemble of 20 structures of the Mg^{2+}-bound DD mutant is shown in Figure 5(A).

The secondary structure elements of the Mg^{2+}-bound form of the DD mutant are essentially identical to those of the apo form and the Ca^{2+}-bound form of the wild type [Fig. 5(B)]. Helices E and F form EF-hand III, and helices G and H form EF-hand IV. The short antiparallel β-sheet connecting EF-hands III and IV is also conserved. The first six residues in the EF-hand III binding sequence and I130-G134 in EF-hand IV were not defined well, due to the lack of medium- and long-range NOEs.

Discussion

Mg^{2+}-induced conformational changes in the EF-hand IV

The Mg^{2+}-induced conformational changes occurred in wide area of EF-hand IV, while the closed conformation was retained. The global fold of the Mg^{2+}-bound form was similar to that of the apo form [Fig. 5(B)]. In particular, the EF-hand III structures were almost identical. For EF-hand III, the backbone R.M.S.D. between the Mg^{2+}-bound and apo forms was 0.85 ± 0.13 Å.

Mg^{2+} binding induced conformational changes in EF-hand IV. Initially, the N-terminal part of the EF-hand IV binding sequence, which directly interacts with Mg^{2+}, was rearranged. In the apo form, the side chain of I130 is buried and interacts with the hydrophobic A128, V136 and F141 residues [Fig. 5(C), left]. In the Mg^{2+}-bound form, D129 occupies this position and forms a hydrogen bond with G134. As a result, I130 was extruded [Fig. 5(C), center]. D129 is an important residue for the coordination to Mg^{2+} or Ca^{2+} on the inside of the molecule [Fig. 5(C), center and right]. As previously mentioned, the hydrogen bond formation by G134 was indicated by the amide signal position [Fig. 1(A)]. This was also observed in the Ca^{2+}-induced changes. The rearrangement of the N-terminal part of the EF-hand IV binding sequence shifted the C-terminus of helix G toward the β-sheet. The backbone of A128 was converted into the regular α-helical conformation in the Mg^{2+}-bound form [Fig. 5(C)]. In association with the movement of D129, A128 was also oriented toward the inside of the molecule, resulting in the extension of the α-helix. As compared to the apo form, the averaged ϕ and ψ angles of A128 changed from −89.3° to −63.9° and from 153.0° to −47.3°, respectively. These changes were also observed in the Ca^{2+}-bound form. Accordingly, helix G was tilted toward the open orientation by approximately 10 degrees, and helix H was also tilted in a similar direction to helix G [Fig. 5(B)]. Consequently, the inter-helical angle between helices G and H in the Mg^{2+}-bound form was close to that in the apo form (Supporting Information Table S4).

Conformational change in the hydrophobic core

The Mg^{2+}-induced changes also occurred in another region, in addition to the postulated Mg^{2+} position. Around the C-terminal end of the EF-hand IV

binding sequence, Y138 and F141 also changed their interaction partners. New aromatic interactions between F89, Y138, and F141 were created in the Mg^{2+}-bound form [Fig. 5(D)]. This may be attributed to the movement of helices G and H. In the apo form, the aromatic ring of Y138 is oriented toward the C-terminus of helix E and the β-sheet.[2–4] In the Mg^{2+}-bound form, the ring is away from the β-sheet and faces F89 vertically [Fig. 5(D)]. The up-field ring current shift observed in the δ proton of Y138 can be attributed to the interaction with F89. The orientation of the ring of F141 changed from helix G to helix F, and was close to V108 on helix F and the aromatic ring of F89 on helix E [Fig. 5(D)]. These conformational changes are also observed in the presence of Ca^{2+}. However, the extents of the structural changes are larger in the Ca^{2+}-bound form, and those of the Mg^{2+}-bound form are around the mid points, as seen in Figure 5(D).

In contrast to the effects of Ca^{2+} binding, the Mg^{2+}-induced structural changes exerted only a minor influence on the inter-helical angles (Supporting Information Table S4). The hydrophobic core, which provides the binding surface for the target molecules, remained buried. The conformation of EF-hand III was minimally affected by Mg^{2+} binding. The Ca^{2+}-induced movements of Y138 and F141 were more significant, as compared to those induced by Mg^{2+}. Taken together, the structure of the Mg^{2+}-bound form can be considered as an intermediate state of the structural changes caused by Ca^{2+} binding.

The incorporation of Mg^{2+} in the binding sequence leads to the formation of ionic interactions between Mg^{2+} and the negatively charged residues. These ionic interactions contribute to the thermal stability of the Mg^{2+}-bound form of CaMC. The hydrogen bond is an additional stabilizing factor. The extension of the C-terminal end of helix G increases the hydrogen bond network, in addition to the hydrogen bond between G134 and D129.

Mg^{2+} coordination

The geometry of the Ca^{2+} coordination can be described as a pentagonal bipyramid, in which six of the seven Ca^{2+} ligands are provided from the residues at positions 1, 3, 5, 7, and 12 (a bidentate ligand). The remaining Ca^{2+} ligand is the residue at position 9, via a water molecule. The Ca^{2+}-induced rearrangements of positions 1, 2, and 6 of the EF-hand IV binding sequence were also found in the Mg^{2+}-bound form, suggesting that the accommodation of Mg^{2+} in this region of the EF-hand IV binding sequence is similar to that of Ca^{2+}, though NMR signal broadening shows dynamic behavior of positions 3 and 5.

The binding of Ca^{2+} or Mg^{2+} induced the shift of the nitrogen resonance of E139 (Supporting Information Table S5), which is one of the largest chemical shift changes. One explanation for the nitrogen resonance shift is the rearrangement of the main-chain structure, but the ϕ and ψ backbone dihedral angles of E139 are minimally affected by Ca^{2+} or Mg^{2+} binding, since E139 is within a helical structure. Another possible reason is hydrogen bond formation. The disruption of the hydrogen bond affects the nitrogen resonance and induces an up-field shift. The crystal structure of the Ca^{2+}-bound form of CaM revealed that no atom is involved in a hydrogen bond with the main-chain amide of E139.[1] In the ensemble of NMR structures of the apo form, the side chain of N137 is located in the vicinity of the E139 main-chain amide, and could potentially form a hydrogen bond.[2–4] Although the crystal structure of the apo form of CaM has not been solved, the corresponding hydrogen bond exists in the crystal structure of the Ca^{2+}-free form of the EF-hand protein, aequorin.[32] Accordingly, a hydrogen bond may exist between the main-chain amide of E139 and the side-chain oxygen of N137 in the apo form of CaM. The hydrogen bond disappears upon Ca^{2+} or Mg^{2+} binding. N137, at position 9 in the binding sequence, uses its side chain to coordinate to Ca^{2+} via a water molecule. As in Ca^{2+} binding, Mg^{2+} binding may involve N137. The disruption of the hydrogen bond to helix H may be related to the neighboring conformational changes, as described above.

Additional features in the wild type Mg^{2+}-bound form

In the structural determination of the Mg^{2+}-bound form of the DD mutant, the structural changes were observed only in EF-hand IV, while in the wild type, the Mg^{2+}-induced broadening ranged from the β-sheet to the core, including EF-hand III. The resonances of the hydrophobic residues at position 8 (I100 and V136) in the binding sequences of EF-hands III and IV were severely broadened in the wild type. The residue at position 8 is located at the center of the β-strand, and links the paired EF-hands structurally. The exchange broadening was also observed in the residues of the hydrophobic core, in the vicinity of the β-sheet region, and the residues between helices E and F (Fig. 6). One explanation for the broadening of the Mg^{2+}-bound form of the wild type is the multiple conformations in the β-sheet region and the surrounding region, including the hydrophobic core. Fewer conformational exchanges in the β-sheet region occurred in the DD mutant. Replacing glutamate with aspartate at position 12 places the carboxylate group farther away from the bound metal, decreasing the population coordinated with the residue at position 12. The DD mutation may have excluded such low-population structures. Mg^{2+} binding only to EF-hand IV can lead to the simultaneous movement of both EF-

hands III and IV, since a low Mg^{2+} concentration produces overall broadening. This implies that a critical mechanism underlying the cooperativity of the two EF-hands is reflected in the Mg^{2+}-induced broadening.

In summary, the Mg^{2+}-induced conformational change mainly occurs on the helix G and helix H sides of the binding sequence of EF-hand IV, and involves the rearrangement of the hydrophobic interactions. The features of the Mg^{2+}-induced conformational changes of CaMC are included in the Ca^{2+}-induced conformational changes. The structure of the Mg^{2+}-bound form can be regarded as an intermediate state of the structural changes caused by Ca^{2+} binding. Therefore, the Ca^{2+}-induced conformational changes of CaMC can be divided into two categories, those specific to Ca^{2+} and those common to Ca^{2+} and Mg^{2+}.

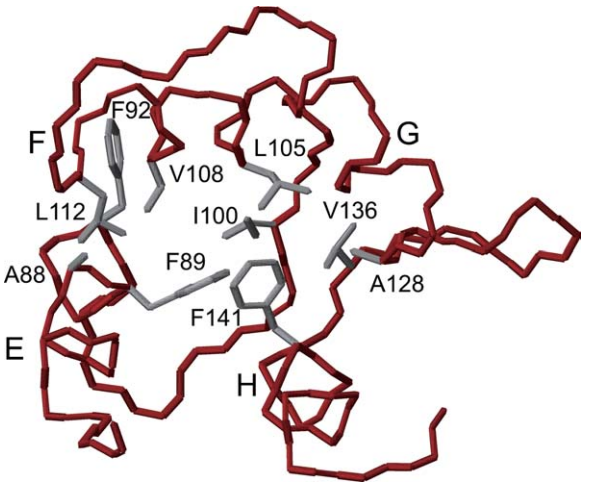

Figure 6. Backbone trace of the Mg^{2+}-bound form of the CaMC DD mutant. The hydrophobic residues with side-chains that undergo exchange broadening in the presence of Mg^{2+} in the wild type are colored grey.

Materials and Methods

Protein expression and purification

For the recombinant expression and purification of CaMC (residues 78-148), the cDNA encoding this region of *Xenopus* CaM was cloned into the pET11a vector (Novagen). The N-terminal methionine was removed naturally. All of the CaM mutants were generated by site-directed mutagenesis, using a QuikChange kit (Stratagene). All unlabeled proteins were expressed in *Escherichia coli* Rosetta2(DE3)pLysS, grown in LB medium at 37 °C. The uniformly ^{15}N or ^{15}N, ^{13}C-labeled proteins were expressed in M9 minimal medium, supplemented with either $^{15}NH_4Cl$ or $^{15}NH_4Cl$ and [$^{13}C_6$]glucose as the sole nitrogen and carbon sources, respectively. The cells were disrupted by sonication, and after clarification by centrifugation, the supernatant was applied to a HiTrap Q FF or HP column (GE Healthcare), in 20 m*M* Tris-HCl (pH 7.5) containing 5 m*M* $CaCl_2$, which was eluted with a NaCl gradient. Fractions containing the protein were applied to a HiTrap Phenyl FF or HP column (GE Healthcare) equilibrated with 20 m*M* Tris-HCl (pH 7.5), containing 5 m*M* $CaCl_2$ and 2.0*M* $(NH_4)_2SO_4$. The column was washed with a buffer containing 20 m*M* Tris-HCl (pH 7.5), 5 m*M* EDTA and 2.0*M* $(NH_4)_2SO_4$. The protein was eluted with a $(NH_4)_2SO_4$ gradient. For dialysis and further sample preparation, Chelex 100-treated 10 m*M* MES (pH 6.5) buffer containing 100 m*M* KCl was used. The fraction containing the protein was dialyzed against 10 m*M* MES (pH 6.5) buffer, containing 100 m*M* KCl. The protein concentration was determined using a molar absorption coefficient of $\varepsilon = 2980\ M^{-1}\ cm^{-1}$.

Hydrophobic interaction chromatography

Hydrophobic interaction chromatography was performed using a 1 mL RESOURCE PHE column (GE Healthcare). The column was equilibrated with an appropriate equilibration buffer, containing 2*M* $(NH_4)_2SO_4$ in 20 m*M* Tris-HCl (pH 7.8). For the apo and Ca^{2+}-loading cases, 5 m*M* EDTA and 5 m*M* $CaCl_2$ were included in the equilibration buffer, respectively. For the Mg^{2+}-loading, either 10 m*M* or 100 m*M* $MgCl_2$ was included in the equilibration buffer. In all experiments, 0.16 mg of the protein was loaded on the column. All experiments were performed at 10°C. Elution was done by decreasing the ammonium sulfate concentration to 0*M* in 20 m*M* Tris-HCl, pH 7.8. The protein eluted under each condition was spectrophotometrically monitored.

NMR measurements and spectral assignments

NMR spectra were measured at 50°C on a Bruker AVANCE600 spectrometer, equipped with pulsed field gradients and triple resonance probes. The samples used in the magnesium titrations initially contained 1 m*M* of ^{15}N-labeled protein, in a buffer consisting of 10 m*M* MES and 100 m*M* KCl in 90% H_2O/10% D_2O, pH 6.5. Small aliquots of a 100 m*M* (1 m*M* to 10 m*M*) or 1*M* (10 m*M* to 100 m*M*) $MgCl_2$ solution were added to the protein solution, and two-dimensional ^1H-^{15}N HSQC spectra were recorded.

Resonance assignments were accomplished by analyses of multidimensional heteronuclear NMR spectra, 2D ^1H-^{15}N HSQC, 2D ^1H-^{13}C HSQC, 3D HNCO, HN(CA)CO, C(CO)NH, HNCACB, CBCA(-CO)NH, HBHA(CO)NH, H(CCO)NH, HCCH-COSY, HCCH-TOCSY and CCH-TOCSY, acquired on a 1 m*M* protein sample (uniformly labeled with ^{13}C and ^{15}N), in buffer containing 10 m*M* MES-d_{13} (pH 6.5), 100 m*M* KCl and 100 m*M* $MgCl_2$ in 90% H_2O/10% D_2O. All spectra were processed using NMRPipe[33] and analyzed using NMRview[34] and the integrated KUJIRA module.[35]

The $^{13}C\alpha$, ^{13}CO secondary shifts were calculated by the table of random coil carbon chemical shifts provided by Wishart and Sykes.[36]

Structure calculations

NOE restraints were obtained from 3D ^{15}N-edited NOESY and ^{13}C-edited NOESY spectra with mixing times of 160 ms. Backbone ϕ and ψ torsion angle restraints were derived from an analysis of the Hα, $^{13}C\alpha$, $^{13}C\beta$, ^{13}CO and backbone ^{15}N chemical shifts using TALOS,[37] including 23 hydrogen bond constraints. The χ^1 angle restraints were derived from the HNHB, HN(CO)HB and NOESY spectra. Automated NOE cross-peak assignments and structure calculations with torsion angle dynamics were performed using CYANA 2.2.[29–31] A total of 100 structures were independently calculated. The 20 conformers with the lowest final CYANA target functions were used. Figures were generated with MOLMOL. The coordinates for the Mg^{2+}-bound CaMC E104D/E140D mutant have been deposited in the Protein Data Bank (PDB ID: 2EQC).

Acknowledgment

We thank Prof. M. Kainosho and Prof. M. Ikura for providing the *Xenopus* calmodulin cDNA.

References

1. Babu YS, Sack JS, Greenhough TJ, Bugg CE, Means AR, Cook WJ (1985) Three-dimensional structure of calmodulin. Nature 315:37–40.
2. Kuboniwa H, Tjandra N, Grzesiek S, Ren H, Klee CB, Bax A (1995) Solution structure of calcium-free calmodulin. Nat Struct Biol 2:768–776.
3. Zhang M, Tanaka T, Ikura M (1995) Calcium-induced conformational transition revealed by the solution structure of apo calmodulin. Nat Struct Biol 2:759–767.
4. Finn BE, Evenäs J, Drakenberg T, Waltho JP, Thulin E, Forsén S (1995) Calcium-induced structural changes and domain autonomy in calmodulin. Nat Struct Biol 2:777–787.
5. Krestinger RH, Nockolds CE (1973) Carp muscle calcium binding protein: structure determination and general description. J Biol Chem 248:3313–3326.
6. Ikura M, Clore GM, Gronenborn AM, Zhu G, Klee CB, Bax A (1992) Solution structure of a calmodulin-target peptide complex by multidimensional NMR. Science 256:632–638.
7. Meador WE, Means AR, Quiocho FA (1992) Target enzyme recognition by calmodulin: 2.4 A structure of a calmodulin-peptide complex. Science 257:1251–1255.
8. Meador WE, Means AR, Quiocho FA (1993) Modulation of calmodulin plasticity in molecular recognition on the basis of x-ray structures. Science 262:1718–1721.
9. Chin D, Means AR (2000) Calmodulin: a prototypical calcium sensor. Trends Cell Biol 10:322–328.
10. Ohki S, Ikura M, Zhang M (1997) Identification of Mg^{2+} binding sites and the role of Mg^{2+} on target recognition by calmodulin. Biochemistry 36:4309–4316.
11. Tsai MD, Drakenberg T, Thulin E, Forsén S (1987) Is the binding of magnesium (II) to calmodulin significant? An investigation by magnesium-25 nuclear magnetic resonance. Biochemistry 26:3635–3643.
12. Seamon KB (1980) Calcium- and magnesium-dependent conformational states of calmodulin as determined by nuclear magnetic resonance. Biochemistry 19: 207–215.
13. Drabikowski W, Brzeska H, Venyaminov S (1982) Tryptic fragments of calmodulin. Ca^{2+}- and Mg^{2+}-induced conformational changes. J Biol Chem 257:11584–11590.
14. Malmendal A, Evenäs J, Thulin E, Gippert GP, Drakenberg T, Forsén S (1998) When size is important. Accommodation of magnesium in a calcium binding regulatory domain. J Biol Chem 273:28994–29001.
15. Ebel H, Gunther T (1980) Magnesium metabolism: a review. J Clin Chem Clin Biochem 18:257–270.
16. Huang H, Ishida H, Vogel HJ (2010) The solution structure of the Mg^{2+} form of soybean calmodulin isoform 4 reveals unique features of plant calmodulins in resting cells. Protein Sci 19:475–485.
17. Masino L, Martin SR, Bayley PM (2000) Ligand binding and thermodynamic stability of a multidomain protein, calmodulin. Protein Sci 9:1519–1529.
18. Brzeska H, Venyaminov S, Grabarek Z, Drabikowski W (1983) Comparative studies on thermostability of calmodulin, skeletal muscle troponin C and their tryptic fragments. FEBS Lett 153:169–173.
19. Lee SH, Kim JC, Lee MS, Heo WD, Seo HY, Yoon HW, Hong JC, Lee SY, Bahk JD, Hwang I, Cho MJ (1995) Identification of a novel divergent calmodulin isoform from soybean which has differential ability to activate calmodulin-dependent enzyme. J Biol Chem 270: 21806–21812.
20. Minowa O, Yagi K (1984) Calcium binding to tryptic fragments of calmodulin. J Biochem 96:1175–1182.
21. Martin SR, Masion L, Bayley PM (2000) Enhancement by Mg^{2+} of domain specificity in Ca^{2+}-dependent interactions of calmodulin with target sequences. Protein Sci 9:2477–2488.
22. Finley NL, Howarth JW, Rosevear PR (2004) Structure of the Mg^{2+}-loaded C-lobe of cardiac troponin C bound to the N-domain of cardiac troponin I: comparison with the Ca^{2+}-loaded structure. Biochemistry 43: 11371–11379.
23. Babini E, Bertini I, Capozzi F, Chirivino E, Luchinat C (2006) A structural and dynamic characterization of the EF-Hand Protein CLSP. Structure 14:1029–1038.
24. Ikura M, Minowa O, Yazawa M, Yagi K, Hikichi K (1987) Sequence-specific assignments of downfield-shifted amide proton resonances of calmodulin. Use of two-dimensional NMR analysis of its tryptic fragments. FEBS Lett 219:17–21.
25. da Silva AC, Kendrick-Jones J, Reinach FC (1995) Determinants of ion specificity on EF-hands sites. Conversion of the Ca^{2+}/Mg^{2+} site of smooth muscle myosin regulatory light chain into a Ca(2+)-specific site. J Biol Chem 270:6773–6778.
26. Blumenschein TM, Reinach FC (2000) Analysis of affinity and specificity in an EF-hand site using double mutant cycles. Biochemistry 39:3603–3610.
27. Cates MS, Berry MB, Ho EL, Li Q, Potter JD, Phillips GN, Jr. (1999) Metal-ion affinity and specificity in EF-hand proteins: coordination geometry and domain plasticity in parvalbumin. Structure 7:1269–1278.
28. Harper ET, Rose GD (1993) Helix stop signals in proteins and peptides: the capping box. Biochemistry 32: 7605–7609.
29. Güntert P (2004) Automated NMR structure calculation with CYANA. Methods Mol Biol 278:353–378.
30. Güntert P, Mumenthaler C, Wüthrich K (1997) Torsion angle dynamics for NMR structure calculation with the new program DYANA. J Mol Biol 273:283–298.

31. Hermann T, Güntert P, Wüthrich K (2002) Protein NMR structure determination with automated NOE assignment using the new software CANDID and the torsion angle dynamics algorithm DYANA. J Mol Biol 319:209–227.
32. Head JF, Inouye S, Teranishi K, Shimomura O (2000) The crystal structure of the photoprotein aequorin at 2.3 A resolution. Nature 405:372–376.
33. Delaglio F, Grzesiek S, Vuister GW, Zhu G, Pfeifer J, Bax A (1995) NMRPipe: a multidimensional spectral processing system based on UNIX pipes. J Biomol NMR 6:277–293.
34. Johnson BA, Blevins RA (1994) NMRView: a computer program for the visualization and analysis of NMR data. J Biomol NMR 4:603–614.
35. Kobayashi N, Iwahara J, Koshiba S, Tomizawa T, Tochio N, Güntert P, Kigawa T, Yokoyama S (2007) KUJIRA, a package of integrated modules for systematic and interactive analysis of NMR data directed to high-throughput NMR structure studies. J Biomol NMR 39:31–52.
36. Wishart DS, Sykes BD (1994) The ^{13}C chemical-shift index: a simple method for the identification of protein secondary structure using ^{13}C chemical-shift data. J Biomol NMR 4:171–180.
37. Cornilescu G, Delaglio F, Bax A (1999) Protein backbone angle restraints from searching a database for chemical shift and sequence homology. J Biomol NMR 13:289–302.